Å range and with the three bridging chlorine atoms at much longer distances between 3.03 (1) and 3.31 (1) Å.
(11) R. C. Weast, Ed., "Handbook of Chemistry and Physics", 49th ed, The Chemical Rubber Co., Cleveland, Ohio, 1968, p B-177.
(12) T. S. Piper, F. A. Cotton, and G. Wilkinson, *J. Inorg. Nucl. Chem.*, **1**, 165 (1955).
(13) We are indebted to Dr. A. S. Foust for running the mass spectra.
(14) Calculations were performed on a UNIVAC 1108 computer. Programs used included original or modified versions of A. S. Foust's ANGSET, E. F. Epstein's DREDGE, J. F. Blount's FOURIER and DEAR, W. R. Busing, K. O. Martin, and H. A. Levy's ORFLS and ORFFE, C. K. Johnson's ORTEP, and D. L. Smith's PLANES.
(15) "International Tables for X-Ray Crystallography", Vol. III, Kynoch Press, Birmingham, England, 1962: (a) p 157; (b) p 215.
(16) $R_1 = |\sum \|F_o| - |F_c\| / \sum |F_o|] \times 100$ and $R_2 = [\sum w_i \|F_o| - |F_c\|^2 / \sum w_i |F_o|^2]^{1/2} \times 100$. All least-squares refinements were based on the minimization of $\sum w_i \|F_o| - |F_c\|^2$ with the individual weights $w_i = 1/\sigma(F_o)^2$.
(17) Atomic scattering factors used are from H. P. Hanson, F. Herman, J. D. Lea, and S. Skillman, *Acta Crystallogr.*, **17**, 1040 (1964). The real and imaginary corrections for anomalous dispersion for Mo Kα radiation applied in the final least-squares cycles are $\Delta f' = -0.6$, $\Delta f'' = 2.0$ for antimony, $\Delta f' = 0.4$, $\Delta f'' = 1.0$ for iron, and $\Delta f' = 0.1$, $\Delta f'' = 0.2$ for chlorine atoms.[15b]
(18) Although Pauling[19a] listed the van der Waals radius for antimony as 2.2 Å which gives the Sb···Cl van der Waals contact the value 4.0 Å, Hulme and Szymanski[4] proposed that this radius for antimony is about 1.8 Å such that the nonbonding Sb···Cl contact should be about 3.6 Å in the molecular complexes.
(19) L. Pauling, "The Nature of the Chemical Bond", 3d ed, Cornell University Press, Ithaca, N.Y., 1960: (a) p 260; (b) pp 246–249.
(20) (a) R. F. Bryan, *J. Chem. Soc. A*, 192 (1967); (b) R. F. Bryan, P. T. Greene, G. A. Melson, P. F. Stokely, and A. R. Manning, *Chem. Commun.*, 722 (1969).
(21) I. Lindquist and A. Niggli, *J. Inorg. Nucl. Chem.*, **2**, 1345 (1956).
(22) G. E. Peterson, Ph.D. Thesis, University of Pittsburgh, 1962.
(23) S. M. Swingle, quoted by P. W. Allen and L. E. Sutton, *Acta Crystallogr.*, **3**, 46 (1959).
(24) P. Kisliuk, *J. Chem. Phys.*, **22**, 86 (1954).
(25) T. Bjorvatten, *Acta Chem. Scand.*, **20**, 1863 (1966).
(26) S. M. Ohlberg, *J. Am. Chem. Soc.*, **81**, 811 (1959).
(27) (a) R. J. Gillespie and R. S. Nyholm, *Q. Rev., Chem. Soc.*, **11**, 339 (1957); (b) R. J. Gillespie, *J. Chem. Educ.*, **47**, 18 (1970); (c) R. J. Gillespie, *ibid.*, **51**, 367 (1974).
(28) R. J. Gillespie, *Angew. Chem., Int. Ed. Engl.*, **6**, 819 (1967).
(29) Of the three arrangements given for seven electron pairs (viz., the 1:3:3 structure, the 1:4:2 structure, and the 1:5:1 or pentagonal-bipyramidal structure),[28] it is presumed from a consideration of the observed environment about each Sb(III) in the 4:4 iron–antimony complex that any steric activity of the lone pair would involve a 1:3:3 arrangement with the lone pair primarily localized along the pseudo-threefold axis in the direction of the bridging chlorine ligands. The closeness of the Cl–Sb–Cl bond angles in this molecular complex to 90° suggests that any steric activity of the lone pair is not appreciable.
(30) D. R. Schroeder and R. A. Jacobson, *Inorg. Chem.*, **12**, 210 (1973).
(31) S. L. Lawton and R. A. Jacobson, *Inorg. Chem.*, **5**, 743 (1966).
(32) S. K. Porter and R. A. Jacobson, *J. Chem. Soc. A*, 1359 (1970).
(33) S. K. Porter and R. A. Jacobson, *J. Chem. Soc. A*, 1356 (1970).
(34) (a) E. E. Aynsley and A. C. Hazell, *Chem. Ind. (London)*, 611 (1963); (b) A. C. Hazell, *Acta Chem. Scand.*, **20**, 165 (1966).
(35) (a) I. D. Brown, *Can. J. Chem.*, **42**, 2758 (1964); (b) A. K. Das and I. D. Brown, *ibid.*, **44**, 939 (1966).
(36) However, it is noteworthy that vibrational spectral data[37] indicate that SbX_6^{3-} and TeX_6^{2-} (X = Cl, Br, I) anions in solution (unlike the solid-state structures) appear to adopt fluxional nonoctahedral configurations not dissimilar from that of the electronically equivalent XeF_6 molecule.[38]
(37) (a) C. J. Adams and A. J. Downs, *Chem. Commun.*, 1699 (1970); (b) J. Milne, *Can. J. Chem.*, **53**, 888 (1975).
(38) (a) R. M. Gavin, Jr., and L. S. Bartell, *J. Chem. Phys.*, **48**, 2460 (1968); (b) L. S. Bartell and R. M. Gavin, Jr., *ibid.*, **48**, 2466 (1968); (c) H. H. Claassen, G. L. Goodman, and H. Kim, *J. Chem. Phys.*, **56**, 5042 (1972).
(39) J. Y. Beach, quoted by L. Pauling, "The Nature of the Chemical Bond", 3d ed, Cornell University Press, Ithaca, N.Y., 1960, p 251.
(40) M. C. Poore and D. R. Russell, *Chem. Commun.*, 18 (1971).

Contribution from the Department of Chemistry, University of California, Riverside, California 92502

Mechanisms of Substitution of Ligand-Bridged Diiron Hexacarbonyl Complexes. μ-Butatriene-bis(tricarbonyliron) Complexes: Crystallographic Determination of the Structure of a Carbonyl Substitution Product and Evidence for a Carbonyl-Inserted Intermediate

J. N. GERLACH,[1a] R. M. WING, and P. C. ELLGEN*[1b]

Received January 13, 1976 AIC60035H

μ-Butatriene-bis(tricarbonyliron) complexes react with phosphines and phosphites to substitute the carbonyl ligand trans to the iron–iron bond. The addition of an incoming ligand without loss of a carbonyl moiety can be demonstrated in some cases by isolation and characterization of the adduct. Such adducts lose carbon monoxide upon heating. Kinetic data are reported for the carbonyl substitution reactions of triphenylphosphine and triphenyl phosphite with μ-butatriene-bis(tricarbonyliron), μ-tetraphenylbutatriene-bis(tricarbonyliron), and μ-di(biphenyl-2,2′-ylidene)-bis(tricarbonyliron) and for the addition without carbonyl displacement of tri-*n*-butylphosphine to μ-tetraphenylbutatriene-bis(tricarbonyliron). The mechanisms of these reactions are discussed. The crystal and molecular structure of one of these products, μ-butatriene-(triphenylphosphine)pentacarbonyldiiron, has been determined by x-ray crystallography. Four molecular units of $Fe_2PO_5C_{27}H_{19}$ (mol wt 566) are distributed in a monoclinic cell ($P2_1/c$) with $a = 11.277$ (4) Å, $b = 13.349$ (6) Å, $c = 17.604$ (7) Å, and $\beta = 107.64$ (1)° and a volume of 2526 Å^3. The structure was refined to a residual of 0.063 (based on F) using 1403 diffractometer-collected reflection intensities. Each iron atom is in an octahedral environment which is completed by an iron–iron bond of 2.627 Å. The bridging butatriene ligand retains a planar carbon skeleton but is twisted end for end by 90° in a manner which suggests π-allyl bonding to each iron atom. The phosphine substituent is observed to be trans to the iron–iron bond.

Introduction

Previous reports document the kinetics and mechanisms of the reactions of organosulfur-,[2] organonitrogen-,[3] and organophosphorus-bridged[4] bis(tricarbonyliron) complexes with Lewis bases. Butatriene–bis(tricarbonyliron) complexes have structures[5] which are similar to the structures of the sulfur-,[6] nitrogen-,[7] and phosphorus-bridged[8] complexes. The structure of di(biphenyl-2,2′-ylidene)butatrienebis(tricarbonyliron),[5] $Fe_2(CO)_6(\mu\text{-}C_{28}H_{16})$, consists of two $Fe(CO)_3$ groups connected by an iron–iron bond as well as by the bridging butatriene group. One interesting feature of the structure is that the ends of the butatriene bridging group extend over one side of the octahedral faces containing the two central butatriene carbon atoms and the carbonyl ligands trans to the iron–iron bond. This feature results from the formation of a π-allylic bond from the butatriene group to each of the iron atoms.

The kinetic data for the nitrogen-[3] and sulfur-bridged[2] complexes can be rationalized by a bimolecular substitution

mechanism in which the activated complex has the entering and leaving groups occupying an edge of an octahedral wedge which is parallel to the edge defined by the two bridging atoms. For steric reasons, such an octahedral wedge cannot be formed by $Fe_2(CO)_6(\mu\text{-}P(C_6H_5)_2)_2$; as a result, carbonyl substitution occurs by a different mechanism.[4] The structure of $Fe_2(CO)_6(\mu\text{-}C_{28}H_{16})$ suggests that steric hindrance to the formation of seven-coordinate activated complexes for butatriene-bridged substrates should be intermediate between that for the nitrogen- or sulfur-bridged complexes and that for the phosphorus-bridged complexes.

Kinetic data for carbonyl substitution are reported for the reactions of triphenylphosphine and triphenyl phosphite with μ-butatriene-bis(tricarbonyliron) (I), μ-tetraphenylbutatriene-bis(tricarbonyliron) (II), and μ-di(biphenyl-2,2′-ylidene)butatriene-bis(tricarbonyliron) (III). Also reported are kinetic data for the reaction of tri-*n*-butylphosphine with II. The products of these reactions and the tri-*n*-butylphosphine derivatives of I and III have been characterized. The crystal and molecular structure of $Fe_2(CO)_5(\mu\text{-}C_4H_4)P(C_6H_5)_3$ has been determined by x-ray crystallography.

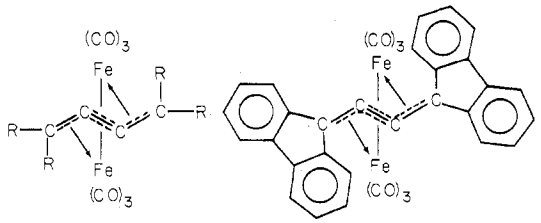

I, R = H
II, R = C_6H_5

III

Experimental Section

Materials and Iron Carbonyl Complexes. Reagent grade solvents were refluxed over calcium hydride and distilled in a nitrogen atmosphere. Diiron nonacarbonyl was prepared by a literature method.[9] Triiron dodecacarbonyl[10] was purified by Soxhlet extraction with pentane. Tetraphenylbutatriene and bis(biphenyl-2,2′-ylidene)butatriene were prepared by reaction of the respective ketones with acetylene Grignard reagent followed by dehydration.[11] Butatrienebis(tricarbonyliron), tetraphenylbutatrienebis(tricarbonyliron), and bis(biphenyl-2,2′-ylidene)butatrienebis(tricarbonyliron) were prepared by a literature method.[12]

Monosubstituted derivatives of the butatriene complexes were prepared by reacting a one-to-one mixture of ligand and substrate at conditions similar to those used in the rate experiments. Reaction products were chromatographed on silica gel, and the derivatives were eluted with benzene–chloroform solutions. Derivatives containing the tri-*n*-butylphosphine ligand were oils. All of the other derivatives were obtained as dark red to black crystals by slow cooling of dichloromethane–hexane solutions. Satisfactory carbon, hydrogen, and iron analyses were obtained (see supplementary material).

Carbonyl region infrared spectra were recorded in chloroform solution and were calibrated vs. indene[13] and polystyrene. Ir (cm^{-1}), ν_{CO}: for $Fe_2(CO)_6C_4H_4$, 2080 s, 2035 s, 2002 vs, 1988 s; for $Fe_2(CO)_6C_4H_4P(n\text{-}C_4H_9)_3$, 2034 s, 1954 s, 1925 m, 1568 m; for $Fe_2(CO)_5C_4H_4P(n\text{-}C_4H_9)_3$, 2034 s, 1954 s, 1925 m; for $Fe_2(CO)_5C_4H_4P(C_6H_5)_3$, 2047 s, 1984 vs, 1960 sh, 1933 w; for $Fe_2(CO)_5C_4H_4P(OC_6H_5)_3$, 2051 s, 1992 vs, 1975 m, 1930 w; for $Fe_2(CO)_6C_{28}H_{16}$, 2069 s, 2038 vs, 2005 s, 1977 w; for $Fe_2(CO)_6C_{28}H_{16}P(n\text{-}C_4H_9)_3$, 2050 s, 1995 vs, 1965 w, 1938 m, 1520 m; for $Fe_2(CO)_5C_{28}H_{16}P(n\text{-}C_4H_9)_3$, 2050 s, 1995 vs, 1965 w, 1938 m; for $Fe_2(CO)_5C_{28}H_{16}P(C_6H_5)_3$, 2049 s, 1992 vs, 1957 vw, 1935 w; for $Fe_2(CO)_5C_{28}H_{16}P(OC_6H_5)_3$, 2055 s, 2000 vs, 1961 vw, 1940 w; for $Fe_2(CO)_6C_4(C_6H_5)_4$, 2066 s, 2033 s, 2000 s, 1984 w; for $Fe_2(CO)_6C_4(C_6H_5)_4P(n\text{-}C_4H_9)_3$, 2043 s, 1990 vs, 1958 w, 1929 m, 1529 m; for $Fe_2(CO)_5C_4(C_6H_5)_4P(n\text{-}C_4H_9)_3$, 2043 s, 1990 vs, 1958 w, 1929 m; for $Fe_2(CO)_5C_4(C_6H_5)_4P(C_6H_5)_3$, 2048 s, 1986 vs, 1962 vw, 1935 w; for $Fe_2(CO)_5C_4(C_6H_5)_4P(OC_6H_5)_3$, 2050 s, 1995 vs, 1970 m, 1933 m.

Instrumentation. Infrared spectra were recorded on a Perkin-Elmer Model 621 spectrometer using an expanded linear wavenumber scale. Mass spectra were obtained on a Finnigan 1015 S/L spectrometer interfaced with a PDP 8/m computer programmed to provide a digital readout of peak intensity.

Rate Measurements. All rate studies were carried out under pseudo-first-order conditions using at least a tenfold excess of ligand. In each case, a stock solution of ligand was diluted to the desired concentration in a Schlenk tube. The tube was placed in a constant-temperature bath, and the ligand solution was purged with carbon monoxide. The reaction was initiated by injection of a 1-ml aliquot of a stock solution of the appropriate iron carbonyl substrate. At appropriate intervals, aliquots were transferred from the reaction mixture to a 1-mm path length infrared cell. A matched reference cell contained a solution of ligand at the same concentration as in the reaction mixture. The disappearance of the highest frequency carbonyl-stretching absorption of the iron carbonyl substrate was followed. In some cases the appearance of the highest frequency carbonyl-stretching absorption of the product was monitored concurrently. In these cases the rate of product appearance was always found to be equal to the rate of substrate disappearance. Reactions were monitored for at least 2 half-lives; at least eight data points were obtained in this time interval.

Crystallography. Slow intermixing of a concentrated chloroform solution of $Fe_2(CO)_5C_4H_4P(C_6H_5)_3$ and hexane gave red crystals. A crystal having dimensions 0.4 × 0.2 × 0.2 mm was used for data collection. The crystal was mounted along the **b** axis which corresponds to the long crystal axis.

Preliminary precession (Mo K$\tilde{\alpha}$) photographs showed the crystal to be monoclinic. From the systematic absences for $h0l$ with $l = 2n + 1$ and $0k0$ with $k = 2n + 1$, the space group was determined to be $P2_1/c$. The unit cell constants, a = 11.277 (4) Å, b = 13.349 (6) Å, c = 17.604 (7) Å, and β = 107.64 (1)°, were determined from a least-squares fit of 12 carefully centered reflections having $2\theta \geq 20°$, using Mo Kα_1 radiation (λ 0.709 26 Å). The crystal density obtained by flotation in CCl_4–H_2CCl_2 mixture was 1.50 g/ml, compared with 1.488 g/ml calculated from the x-ray data and a molecular weight of 566, assuming 4 formula units per unit cell.

Intensity data were collected under computer control using a Picker Model FACS four-circle diffractometer with a 32.0-cm crystal to scintillation detector distance and the pulse height analyzer adjusted to accept 90% of the Kα_1 intensity from the 004 reflection. Mo K$\tilde{\alpha}$ radiation was made monochromatic by Bragg reflection from a graphite crystal. Reflections with 2θ values from 3 to 35° were collected for one quadrant of reciprocal space using the 2θ–θ scan technique with a scan rate of 1°/min and scan range of (1.80 + 0.692 tan θ)° and keeping the maximum count rates less than 30000 counts/s to ensure linearity of the integrated intensities. Stationary-counter background counts of 10 s were taken before and after each scan. As a check for electronic and crystal stability during the period of data collection, the intensities of three standard reflections were measured after every 50 reflections, and they showed a random statistical fluctuation of ±5% from the mean. Realignment of the crystal after 900 reflections were collected resulted in no significant change in the intensities of the standard reflections. Altogether, 1953 independent reflections were collected, and of these the 1403 reflections which obeyed the condition $F_o^2 > 1.5\sigma(F_o^2)$ were retained for use in the structure determination. The data were corrected for Lorentz and polarization effects, but absorption was ignored since the linear absorption coefficient is 12.74 cm^{-1} and the range of transmission factors is estimated to be 0.65–0.60.

Solution and Refinement of Structure. The structure was solved by the heavy-atom method. A three-dimensional Patterson map was calculated,[14] from which the positions of the two iron atoms were deduced. After one cycle of least-squares refinement[15] to improve the coordinates of the iron atoms, a difference electron density map was calculated.[16] This resulted in the location of all nonhydrogen atoms with the exception of several carbons in one phenyl ring.

After three cycles of full-matrix least-squares refinement with isotropic thermal parameters and rigid-group treatment of the phenyl groups, a second electron density map revealed the correct orientation of the third phenyl ring. This was followed by one more cycle of least-squares refinement; then the iron and phosphorus atoms were allowed to vibrate anisotropically and the atomic scattering power of iron was corrected for the real and imaginary part of the anomalous dispersion.[17] After two more cycles of least-squares refinement, the individual carbon atoms in each phenyl group were refined with isotropic thermal parameters. Two more cycles of least-squares

refinement were carried out, after which a third difference electron density map revealed the location of the butatriene hydrogens as the largest peaks having $\Delta\rho = 0.6$ e/Å^3. Two cycles of least-squares refinement in which hydrogen atoms were added to each phenyl rigid group and the positional parameters of the butatriene hydrogens were included, followed by an additional cycle of refinement for the terminal butatriene carbon and hydrogen atoms, resulted in final residuals[18] $R_1 = 0.063$ and $R_2 = 0.057$. The maximum parameter shifts in the last two cycles of full-matrix least-squares were 0.6 of the corresponding parameter standard deviation (estimated from the diagonal elements of the inverse matrix), and χ for the fitted data, $[\sum w(F_o - F_c)^2/(m - s)]^{1/2}$ where m is the number of reflections used and $s = 147$ is the number of parameters refined, was 1.23. The calculated and observed structure factors are listed in Table I (supplementary material); the final positional and thermal parameters are given in Table II.

Description and Discussion of the Structure

The crystal structure of $Fe_2(CO)_5C_4H_4P(C_6H_5)_3$ was determined by x-ray diffraction. Two stereoscopic views of $Fe_2(CO)_5C_4H_4P(C_6H_5)_3$ and the numbering of the atoms are shown in Figure 1. For clarity, the phosphine phenyl rings have been omitted, and the butatriene carbons have been designated with a "B" in Figure 1.

The coordination geometry about each iron atom is best described as a distorted octahedron. The Fe_1–Fe_2 distance of 2.63 Å establishes the presence of an iron–iron bond.[19] The phosphine is coordinated trans to the iron–iron bond. Thus, the position of substitution is the same as that observed for the nitrogen-,[3,20] phosphorus-,[4] and sulfur-bridged[2] complexes.

The structure of the butatriene group is distorted from that of free butatriene, which is linear. This distortion results from the formation of a π-allyl bond to each iron atom. The addition of three electrons from a π-allyl bond provides each iron atom with an inert-gas configuration of 36 electrons. Formation of an iron–iron bond results in distortion of the bonding between the iron and the π-allyl moiety. Thus, the Fe_1–B_2 (1.95 Å) and Fe_1–B_3 (2.21 Å) bond lengths are not identical but represent a compromise between the need for an iron–iron bond and an iron–π-allyl bond. The bonding of the butatriene group to the two iron atoms by π-allyl bonds is further established by the Fe_1–B_1–Fe_2 and Fe_1–B_2–Fe_2 angles of 82.8° (reduced from an ideal 90° by the iron–iron bond) and a dihedral angle of 90° between the two CH_2 groups. As a result, six π-type orbitals of the butatriene are correctly oriented so that they can be combined into two iron–π-allyl bonds.

A comparison of the bond angles (Table III) about each iron atom shows that they are in almost identical environments. This symmetry is the most important feature of the structure. That is, the substitution of a carbonyl ligand by triphenylphosphine has not distorted the molecule. Since triphenylphosphine is much larger than carbon monoxide, this implies that a significant amount of open space exists around the carbonyls trans to the iron–iron bond (see below).

A comparison of this structure with those of $Fe_2(CO)_6(\mu\text{-}SC_2H_5)_2$,[6] $Fe_2(CO)_6(\mu\text{-}N_2C_{12}H_8)$,[7] $Fe_2(CO)_6(\mu\text{-}OC(NC_6H_5)_2)$,[7] and $Fe_2(CO)_6(\mu\text{-}C_{28}H_{16})$[5] shows that the $Fe_2(CO)_6$ moieties have substantially the same geometries in all of these complexes.

See Tables IV and V for intramolecular bond lengths and least-squares planes.

Discussion of the Carbonyl Substitution Mechanism

The reactions of I, II, and III with large excesses of phosphines and phosphites exhibit good pseudo-first-order kinetics. The pseudo-first-order rate constants (Table VI (supplementary material)) for these reactions were obtained by monitoring infrared spectra of reaction mixtures. In all cases, the reactions go to completion and result in the formation of a single product. However, two distinct kinds of reaction product are observed. Depending on the identity of

Table II. Positional and Thermal Parameters in $Fe_2(CO)_5C_4H_4P(C_6H_5)_3$[a]

Atom	x	y	z	B_{11}
Fe_1	0.0759 (2)	0.1390 (1)	0.1478 (1)	113 (2)[b]
Fe_2	0.2000 (1)	0.3007 (1)	0.1335 (1)	81 (2)[c]
P	0.3318 (3)	0.4255 (2)	0.1828 (2)	77 (4)[d]
C_1	0.0620 (13)	0.0206 (13)	0.1897 (9)	8.7 (4)
O_1	0.0493 (10)	−0.0529 (9)	0.2163 (6)	11.7 (3)
C_2	0.1001 (12)	0.0972 (11)	0.0602 (9)	7.0 (4)
O_2	0.1206 (8)	0.0683 (7)	0.0034 (6)	8.2 (3)
C_3	−0.0820 (13)	0.1664 (10)	0.1072 (7)	5.8 (3)
O_3	−0.1883 (9)	0.1859 (7)	0.0820 (5)	7.3 (2)
C_4	0.2014 (10)	0.3037 (9)	0.0347 (7)	5.3 (3)
O_4	0.1988 (7)	0.3053 (6)	−0.0318 (5)	6.3 (2)
C_5	0.0658 (10)	0.3700 (9)	0.1193 (6)	4.2 (3)
O_5	−0.0239 (8)	0.4175 (6)	0.1118 (4)	5.8 (2)
B_1	0.1825 (10)	0.2367 (8)	0.2285 (6)	3.3 (3)
B_2	0.2503 (10)	0.1730 (8)	0.1971 (6)	3.4 (3)
B_3	0.0898 (10)	0.2171 (9)	0.2607 (6)	4.4 (3)
B_4	0.3541 (10)	0.1927 (10)	0.1746 (7)	4.7 (3)
H_1	0.021 (9)	0.253 (8)	0.256 (6)	*e*
H_2	0.101 (9)	0.159 (8)	0.299 (6)	*e*
H_3	0.363 (9)	0.155 (8)	0.134 (6)	*f*
H_4	0.425 (9)	0.229 (8)	0.215 (6)	*f*
		Rigid Groups		
		Phenyl I		
C_1	0.4077 (5)	0.4120 (4)	0.2895 (3)	3.4 (3)
C_2	0.3330 (5)	0.4076 (4)	0.3398 (3)	4.5 (3)
C_3	0.3871 (5)	0.3924 (4)	0.4216 (3)	5.0 (3)
C_4	0.5159 (5)	0.3817 (4)	0.4529 (3)	5.7 (3)
C_5	0.5906 (5)	0.3861 (4)	0.4026 (3)	6.6 (4)
C_6	0.5365 (5)	0.4012 (4)	0.3208 (3)	5.4 (3)
H_2	0.2331	0.4160	0.3155	*g*
H_3	0.3291	0.3890	0.4606	*g*
H_4	0.5579	0.3699	0.5163	*g*
H_5	0.6906	0.3777	0.4269	*g*
H_6	0.5945	0.4047	0.2818	*g*
		Phenyl II		
C_1	0.2627 (5)	0.5506 (9)	0.1738 (9)	3.8 (3)
C_2	0.1904 (5)	0.5792 (9)	0.0975 (9)	4.4 (3)
C_3	0.1404 (5)	0.6757 (9)	0.0844 (9)	5.4 (3)
C_4	0.1628 (5)	0.7436 (9)	0.1476 (9)	5.7 (3)
C_5	0.2351 (5)	0.7149 (9)	0.2239 (9)	5.0 (3)
C_6	0.2850 (5)	0.6184 (9)	0.2370 (9)	4.5 (3)
H_2	0.1730	0.5265	0.0485	*g*
H_3	0.0843	0.6979	0.0252	*g*
H_4	0.1240	0.8184	0.1374	*g*
H_5	0.2524	0.7676	0.2729	*g*
H_6	0.3411	0.5962	0.2961	*g*
		Phenyl III		
C_1	0.4596 (6)	0.4467 (4)	0.1413 (3)	3.8 (3)
C_2	0.5014 (5)	0.3699 (5)	0.1019 (3)	5.7 (3)
C_3	0.6020 (5)	0.3864 (5)	0.0728 (3)	5.8 (3)
C_4	0.6608 (6)	0.4797 (4)	0.0830 (3)	5.7 (3)
C_5	0.6190 (5)	0.5565 (5)	0.1224 (3)	6.0 (3)
C_6	0.5184 (5)	0.5400 (5)	0.1515 (3)	4.9 (3)
H_2	0.4557	0.2975	0.0940	*g*
H_3	0.6344	0.3268	0.0422	*g*
H_4	0.7389	0.4924	0.0604	*g*
H_5	0.6647	0.6289	0.1303	*g*
H_6	0.4860	0.5996	0.1821	*g*

[a] Standard deviations given in parentheses are in the least significant digit. The form of the anisotropic thermal ellipsoid is $\exp[-(B_{11}h^2 + B_{22}k^2 + B_{33}l^2 + 2B_{12}hk + 2B_{13}hl + 2B_{23}kl)]$ and the anisotropic B values have been scaled times 10^4. The units of the isotropic thermal parameters are Å^2. [b] For Fe_1 the thermal parameters $B_{22}, B_{33}, B_{12}, B_{13}$, and B_{23} are 49 (1), 34 (1), −12 (1), 20 (1), and −4 (1), respectively. [c] For Fe_2 the thermal parameters $B_{22}, B_{33}, B_{12}, B_{13}$, and B_{23} are 50 (1), 26 (1), −1 (1), 10 (1), and 0 (1), respectively. [d] For P, the thermal parameters B_{22}, B_{33}, B_{12}, B_{13}, and B_{23} are 56 (3), 24 (1), 1 (3), 9 (2), and −1 (2), respectively. [e] H_1 and H_4 were given the same isotropic temperature factor as that found for B_3. [f] H_3 and H_4 were given the same isotropic temperature factor as that found for B_4. [g] Phenyl hydrogens were given the same isotropic temperature factors as those of the carbon atoms to which they were attached.

Table III. Intramolecular Bond Angles (deg)

Fe_1-Fe_2-P	152.8 (2)	C_1-Fe_1-C_3	98.6 (7)
Fe_2-Fe_1-C_1	152.9 (7)	C_2-Fe_1-B_2	93.5 (6)
Fe_1-Fe_2-C_4	106.3 (5)	C_2-Fe_1-C_3	96.8 (7)
Fe_2-Fe_1-C_2	87.0 (6)	C_3-Fe_1-B_1	117.8 (6)
Fe_1-Fe_2-C_5	89.1 (5)	C_3-Fe_1-B_3	93.2 (6)
Fe_2-Fe_1-C_3	107.2 (6)	P-Fe_2-B_1	102.9 (4)
Fe_1-Fe_2-B_1	50.1 (4)	P-Fe_2-B_2	111.8 (4)
Fe_2-Fe_1-B_1	47.1 (4)	P-Fe_2-B_4	89.7 (5)
Fe_1-Fe_2-B_2	47.4 (4)	P-Fe_2-C_4	99.5 (5)
Fe_2-Fe_1-B_2	49.9 (4)	P-Fe_2-C_5	96.3 (5)
Fe_2-Fe_1-B_3	78.7 (5)	C_4-Fe_2-B_2	119.0 (6)
Fe_1-Fe_2-B_4	79.7 (5)	C_4-Fe_2-B_4	95.7 (6)
		C_4-Fe_2-C_5	96.6 (6)
B_1-Fe_1-B_2	40.1 (5)	C_5-Fe_2-B_1	92.7 (6)
B_2-Fe_2-B_2	40.3 (5)	Fe_1-C_1-O_1	178 (1)
B_1-Fe_1-B_3	37.1 (5)	Fe_1-C_2-O_2	177 (1)
B_2-Fe_2-B_4	37.5 (6)	Fe_1-C_3-O_3	178 (1)
B_2-Fe_1-B_3	72.7 (5)	Fe_2-C_4-O_4	178 (1)
B_1-Fe_2-B_4	72.8 (6)	Fe_2-C_5-O_5	178 (1)
Fe_1-B_1-Fe_2	82.8 (5)		
Fe_1-B_2-Fe_2	82.8 (5)	B_3-B_1-B_2	130.1 (9)
		B_1-B_2-B_4	128.9 (9)
C_1-Fe_1-B_1	113.0 (7)	B_1-B_3-H_1	128 (4)
C_1-Fe_1-B_2	103.2 (7)	B_1-B_3-H_2	118 (4)
C_1-Fe_1-B_3	92.2 (7)	B_2-B_4-H_3	116 (4)
C_1-Fe_1-C_2	98.1 (7)	B_2-B_4-H_4	117 (4)

Table IV. Intramolecular Bond Lengths (Å)

Fe_1-Fe_2	2.627 (3)	C_1-O_1	1.116 (21)
Fe_1-C_1	1.771 (17)	C_2-O_2	1.159 (19)
Fe_1-C_2	1.737 (16)	C_3-O_3	1.175 (16)
Fe_1-C_3	1.746 (13)	C_4-O_4	1.163 (16)
Fe_2-C_4	1.743 (14)	C_5-O_5	1.168 (15)
Fe_2-C_5	1.726 (12)	B_1-B_2	1.367 (17)
Fe_2-P	2.226 (4)	B_1-B_3	1.358 (18)
Fe_1-B_1	2.033 (10)	B_2-B_4	1.370 (18)
Fe_1-B_2	1.948 (11)	B_3-H_1	0.89 (11)
Fe_1-B_3	2.208 (13)	B_3-H_2	1.01 (10)
Fe_2-B_1	1.940 (11)	B_4-H_3	0.90 (11)
Fe_2-B_2	2.025 (10)	B_4-H_4	1.01 (9)
Fe_2-B_4	2.205 (12)		

[a] The numbers in parentheses are the calculated standard deviations in the last significant digits.

Table V. Least-Squares Planes in $Fe_2(CO)_5C_4H_4P(C_6H_5)_3$ and Deviations of Atoms (in Å) from Planes[a]

Atom	Plane I[b]	Plane II	Plane III
B_1	0.046 (10)	−0.006 (10)	
B_2	0.043 (10)		−0.021 (10)
B_3	−0.045 (11)	0.022 (11)	
B_4	−0.044 (11)		0.086 (12)
H_1		−0.009 (100)	
H_2		−0.007 (96)	
H_3			−0.034 (103)
H_4			−0.031 (98)
Rms Δ	0.044 (10)	0.013 (70)	0.049 (72)

The dihedral angle between plane II and plane III is 89.8°

[a] Atoms used in the calculation of planes are indicated. Standard deviations in the least significant digit are given in parentheses. [b] The equations of the least-squares planes are of the form $LX + MY + NZ + D$. The coefficients L, M, N, and D for these planes are, respectively, as follows: plane I, −0.3682, 0.1672, −0.9146, −3.3332; plane II, −0.2424, −0.5834, −0.7752, −5.0128; plane III, −0.2396, 0.8084, −0.5377, −0.3153.

the attacking ligand, carbonyl elimination may (eq 1) or may

$$Fe_2(CO)_6C_4H_4 + L \rightarrow Fe_2(CO)_5C_4H_4L + CO \quad (1)$$

not (eq 2) occur. The pseudo-first-order rate constants for

$$Fe_2(CO)_6C_4H_4 + L \rightarrow Fe_2(CO)_6C_4H_4L \quad (2)$$

the reaction of I with $P(C_6H_5)_3$ and $P(OC_6H_5)_3$ (according to eq 1) are directly proportional to the concentration of the incoming ligand. Hence, the rate law is first-order in each reactant (eq 3).

Table VII. First-Order Rate Constants for Carbonyl Substitution Reactions of Butatrienediiron Hexacarbonyl Complexes[a]

Ligand	10^5k, s^{-1}	T, °C
	$Fe_2(CO)_6C_{28}H_{16}$	
$P(C_6H_5)_3$	4 (1)	110
	17 (1)	120
$P(OC_6H_5)_3$	4 (1)	110
	$Fe_2(CO)_6C_4(C_6H_5)_4$	
$P(C_6H_5)_3$	1.2 (3)	110
	3.2 (3)	120
	9.8 (3)	130
$P(OC_6H_5)_3$	1 (1)	110
	3 (1)	120

[a] First-order rate constants are the values of the intercepts obtained at zero ligand concentration on a plot of k_{obsd} vs. concentration.

Table VIII. Activation Parameters[a] for Carbon Monoxide Dissociation from Ligand-Bridged Diiron Hexacarbonyl Complexes

Complex	$\Delta S^{\ddagger}$, kcal/mol	$\Delta S^{\ddagger}$, cal/(deg mol)
$Fe_2(CO)_6(\mu\text{-}C_4(C_6H_5)_4)$[b]	32 (2)	40 (5)
$Fe_2(CO)_6(\mu\text{-}P(C_6H_5)_2)_2$[c]	37 (2)	10 (4)
$Fe_2(CO)_5(\mu\text{-}SC_6H_5)_2P(C_6H_5)_3$[d]	35.5 (7)	16 (2)

[a] Decalin solution. $P(C_6H_5)_3$ was the incoming ligand in all cases. [b] This work. See Table VII. [c] Reference 4. [d] Reference 21.

$$-d[I]/dt = k[I][L] \quad (3)$$

The reactions of II and III with $P(C_6H_5)_3$ and $P(OC_6H_5)_3$ result in the same types of products as are observed for the reactions of I. However, these reactions are kinetically more complex. For any of these cases, a plot of pseudo-first-order rate constant vs. ligand concentration is linear, with a positive intercept. The slope of the plot is directly proportional to the concentration of the incoming ligand. The value of the intercept at any given temperature is the same for both incoming ligands (see Table VII). These results imply a rate law which contains both a first- and a second-order term (eq 4). In all

$$-d[\text{substrate}]/dt = (k_1 + k_2[L])[\text{substrate}] \quad (4)$$

cases, only one product is observed, indicating that the same carbonyl ligand is substituted by two kinetically different pathways.

The first-order term in eq 4 probably corresponds to a reaction pathway in which the rate-determining step is the rupture of an iron–carbonyl bond to give an intermediate of reduced coordination number. The substitution product is then formed by rapid addition of the incoming group to the intermediate (an SN1 or D mechanism). Similar dissociative mechanisms have been observed for two similar substrates, $(OC)_3Fe(\mu\text{-}P(C_6H_5)_2)Fe(CO)_3$[4] and $(OC)_3Fe(\mu\text{-}SC_6H_5)_2Fe(CO)_2P(C_6H_5)_3$.[21] In both of these cases, steric hindrance to nucleophilic attack at iron in the $Fe(CO)_3$ moiety appears to determine the reaction mechanism. Activation parameters are given in Table VIII for carbonyl dissociation from these substrates and from II. The values are similar.

The second-order term in eq 4 probably corresponds to a reaction pathway in which an unstable intermediate adduct is formed; a simple interpretation is that iron–phosphorus bond making proceeds simultaneously with the insertion of a carbonyl ligand into an iron–butatriene carbon bond (see below). In addition to the rate law and the activation parameters (see Table IX), other features of the data suggest an important role for bond making in the activation process. Thus, the relative rate constants for the reactions studied are consistent with the assumptions that bulky bridging ligands and bulky incoming groups both slow the reaction and that

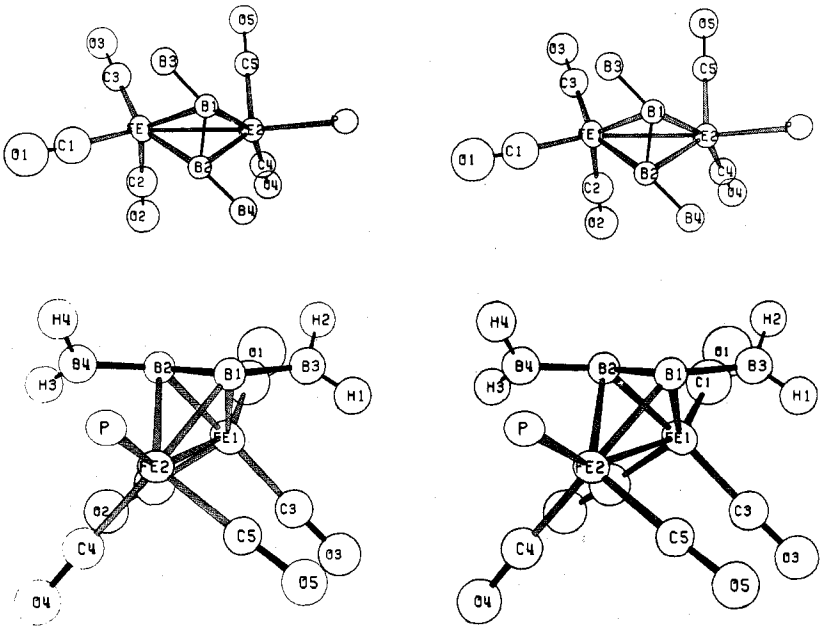

Figure 1. Two stereoscopic views of $Fe_2(CO)_5C_4H_4P(C_6H_5)_3$. The butatriene carbon atoms are labeled with a "B" and the phenyl rings on the phosphine have been omitted.

increased basicity of the incoming ligand speeds the reaction. While it would require a more extensive kinetic study to independently establish the truth of each of these assumptions for butatriene-bridged diiron hexacarbonyl systems, the available kinetic data are wholly consistent with this model. Moreover, strong independent evidence for each of these assumptions has been obtained for similar reactions in closely related systems.[2-4]

A comparison of the second-order rate constants (Table IX) reveals that the order of reactivity is III > I > II when $P(C_6H_5)_3$ is the entering ligand and III > II > I when $P(OC_6H_5)_3$ is the entering ligand. These differences in reactivity cannot be entirely due to steric differences in the butatriene bridging groups, because the order of steric hindrance for the substrates would be expected to be II > III > I. However, this order of steric hindrance does account for the observed difference in reactivity between $P(C_6H_5)_3$ and $P(OC_6H_5)_3$ with these substrates. Triphenylphosphine reacts at a faster rate than triphenyl phosphite with I, at about the same rate with III, and at a much slower rate with II.

Triphenylphosphine is more basic than triphenyl phosphite, and it is expected to be the stronger nucleophile toward these substrates.[2,3] However, the cone angle[22] of $P(OC_6H_5)_3$ is smaller than that of $P(C_6H_5)_3$; that is, the steric requirement of $P(OC_6H_5)_3$ is less than that of $P(C_6H_5)_3$. Therefore, in a case of high steric hindrance, as for II, triphenyl phosphite would react at a much greater rate in comparison to triphenylphosphine than would be expected on the basis of their relative basicities. The fact that III always reacts fastest must be attributed to an electronic effect. The apparent order of electronic influence on reactivity is III > II > I.

The reactions of I, II, and III with $P(n\text{-}C_4H_9)_3$ obey eq 2. One molecule of $P(n\text{-}C_4H_9)_3$ adds to these substrates without displacing a molecule of carbon monoxide. Over the available temperature range, the reaction of $P(n\text{-}C_4H_9)_3$ with I and III is too rapid to permit quantitative rate studies. However, the reaction of II with $P(n\text{-}C_4H_9)_3$ exhibits excellent pseudo-first-order kinetics. The pseudo-first-order rate constants are directly proportional to the concentration of $P(n\text{-}C_4H_9)_3$; the second-order rate law is first order in both substrate and entering ligand (eq 3). Thus, the rate law for the tri-*n*-butylphosphine reaction is the same as that for the triphenylphosphine and triphenyl phosphite reactions, despite the fact that the former reacts according to eq 2, whereas the latter reacts according to eq 1. Activation entropies are also similar for all three incoming groups. The substantial rate differences are reflected only in the activation enthalpies.

Heating the initially formed tri-*n*-butylphosphine derivatives of these butatriene-bridged complexes evolves 1 equiv of carbon monoxide. Since the temperature at which carbon monoxide is evolved is lower than the temperature needed for the reaction of triphenylphosphine or triphenyl phosphite with the butatriene-bridged substrates, it is likely that all of the second-order

Table IX. Second-Order Rate Constants and Activation Parameters for Carbonyl Substitution Reactions of Butatrienediiron Hexacarbonyl Complexes[a]

Ligand	10^3k, M^{-1} s^{-1}	T, °C	$\Delta H^{\ddagger}$, kcal/mol	$\Delta S^{\ddagger}$, cal/(deg mol)
	$Fe_2(CO)_6C_4H_4$			
$P(C_6H_5)_3$	0.119 (5)	80		
	0.22 (1)	90	16 (1)	−32 (2)
	0.42 (2)	100		
$P(OC_6H_5)_3$	0.118 (7)	100		
	0.24 (1)	110	20 (1)	−24 (2)
	0.49 (2)	120		
	$Fe_2(CO)_6C_{28}H_{16}$			
$P(C_6H_5)_3$	2.8 (1)	100		
	4.6 (1)	110	14 (1)	−32 (1)
	7.5 (3)	120		
$P(OC_6H_5)_3$	1.05 (9)	90		
	2.0 (2)	100	16 (1)	−27 (3)
	3.6 (2)	110		
	$Fe_2(CO)_6C_4(C_6H_5)_4$			
$P(C_6H_5)_3$	0.10 (1)	100		
	0.21 (1)	110	24 (1)	−15 (4)
	0.54 (4)	120		
	1.20 (6)	130		
$P(OC_6H_5)$	0.34 (2)	100		
	0.66	110	17 (1)	−29 (3)
	1.15 (5)	120		
$P(n\text{-}C_4H_9)_3$	1.98 (6)	40		
	4.0 (1)	50	13 (1)	−30 (3)
	7.3 (2)	60		
	$Fe_2(CO)_6C_4H_4P(n\text{-}C_4H_9)_3$			
$P(n\text{-}C_4H_9)_3$	1.87 (5)	60		

[a] Decalin solution.

reactions proceed via an intermediate phosphine adduct which still contains all six of the original carbonyl moieties. That is, the product in which the carbonyl ligand is retained is probably present as a transitory intermediate in the other reactions.

Although other formulations cannot be excluded, both the infrared spectra and the mass spectra of the initially formed tri-*n*-butylphosphine adducts are consistent with a structure in which a carbon monoxide ligand inserts between the iron atom and one of the butatriene carbon atoms. Thus the tri-*n*-butylphosphine adducts have a strong infrared absorption in the 1520–1570-cm^{-1} region. With the exception of this band, the carbonyl-region infrared spectra of these adducts are essentially identical with those of the triphenylphosphine and triphenyl phosphite derivatives.

The mass spectra of the tri-*n*-butylphosphine adducts confirm their formulation as $Fe_2(CO)_6C_4H_4P(n\text{-}C_4H_9)_3$, $Fe_2(CO)_6C_{28}H_{16}P(n\text{-}C_4H_9)_3$, and $Fe_2(CO)_6C_4(C_6H_5)_4P(n\text{-}C_4H_9)_3$. In each of these cases, a strong parent peak is observed, and other strong mass peaks correspond to stepwise losses of six carbonyl moieties. This agrees with the generalization[23] that the most common high molecular weight fragments from metal carbonyl complexes typically result from successive losses of carbonyl ligands.

The observations made here for carbonyl substitution reactions of butatriene-bridged diiron hexacarbonyl complexes are paralleled by observations made for the reaction of $(\eta^5\text{-}C_5H_5)Fe(CO)_2CH_3$ with triphenylphosphine,[24] where two products are isolated: $(\eta^5\text{-}C_5H_5)Fe(CO)CH_3P(C_6H_5)_3$ and $(\eta^5\text{-}C_5H_5)Fe(CO)(C(O)CH_3)P(C_6H_5)_3$. The acyl carbonyl in the latter complex gives rise to an infrared band at 1600 cm^{-1}. On being heated, the acyl complex decarbonylates to the methyl complex.

An SN2 carbonyl substitution mechanism for organosulfur-[2] and organonitrogen-bridged[3] diiron hexacarbonyl complexes has been proposed, in which the activated complex contains a seven-coordinate iron atom. A speculative but plausible structure for this activated complex is an octahedral wedge,[25] in which the entering and leaving groups lie on an edge which is parallel to the edge defined by the bridging ligand(s). The kinetic data for the second-order substitution pathway of the butatriene-bridged complexes are consistent with a similar mechanism for this reaction. However, in these cases, the formation of an acyl intermediate by insertion of the "leaving" carbonyl group into an iron–butatriene carbon bond provides a reduced energy pathway for the substitution reaction.

Registry No. $Fe_2(CO)_6C_4H_4$, 12211-98-2; $Fe_2(CO)_6C_4H_4P(n\text{-}C_4H_9)_3$, 60363-55-5; $Fe_2(CO)_5C_4H_4P(n\text{-}C_4H_9)_3$, 60363-56-6; $Fe_2(CO)_5C_4H_4P(C_6H_5)_3$, 60363-57-7; $Fe_2(CO)_5C_4H_4P(OC_6H_5)_3$, 60363-58-8; $Fe_2(CO)_6C_{28}H_{16}$, 41453-35-4; $Fe_2(CO)_6C_{28}H_{16}P(n\text{-}C_4H_9)_3$, 60363-59-9; $Fe_2(CO)_5C_{28}H_{16}P(n\text{-}C_4H_9)_3$, 60363-60-2; $Fe_2(CO)_5C_{28}H_{16}P(C_6H_5)_3$, 60363-61-3; $Fe_2(CO)_5C_{28}H_{16}P(OC_6H_5)_3$, 60363-62-4; $Fe_2(CO)_6C_4(C_6H_5)_4$, 41395-54-4; $Fe_2(CO)_6C_4(C_6H_5)_4P(n\text{-}C_4H_9)_3$, 60363-63-5; $Fe_2(CO)_5C_4(C_6H_5)_4P(n\text{-}C_4H_9)_3$, 60363-64-6; $Fe_2(CO)_5C_4(C_6H_5)_4P(C_6H_5)_3$, 60363-65-7; $Fe_2(CO)_5C_4(C_6H_5)_4P(OC_6H_5)_3$, 60363-66-8; $Fe_2(CO)_6S_2C_6H_3CH_3$, 19964-06-8; $Fe_2(CO)_6S_2C_2H_4$, 15492-14-5; $Fe_2(CO)_6(SC_6H_5)_2$, 15634-63-6; $Fe_2(CO)_6(SC_2H_5)_2$, 15634-62-5; $Fe_2(CO)_6(SCH_2C_6H_5)_2$, 41543-24-2; $Fe_2(CO)_6(SC_4H_4CH_3)_2$, 60363-67-9; $Fe_2(CO)_6N_2(CO)(C_6H_5)_2$, 20935-93-7; $Fe_2(CO)_5N_2(CO)(C_6H_5)_2P(C_6H_5)_3$, 51472-26-5; $Fe_2(CO)_5N_2(CO)(C_6H_5)_2P(OC_6H_5)_3$, 51472-27-6; $Fe_2(CO)_6N_2(CO)(C_6H_4OCH_3)_2$, 51472-19-6; $Fe_2(CO)_5N_2(CO)(C_6H_4OCH_3)_2P(C_6H_5)_3$, 51472-20-9; $Fe_2(CO)_5N_2(CO)(C_6H_4OCH_3)_2P(C_2H_5)(C_6H_5)_2$, 51472-22-1; $Fe_2(CO)_5N_2(CO)(C_6H_4OCH_3)_2P(OC_6H_5)_3$, 51472-21-0; $Fe_2(CO)_5N_2(CO)(C_6H_4OCH_3)_2P(OCH_3)_3$, 51472-25-4; $Fe_2(CO)_5N_2(CO)(C_6H_4OCH_3)_2P(n\text{-}C_4H_9)_3$, 51472-23-2; $Fe_2(CO)_5(P(C_6H_5)_2)_2P(C_6H_5)_3$, 58409-41-9.

Supplementary Material Available: Table I listing calculated and observed structure factors for $Fe_2(CO)_5C_4H_4P(C_6H_5)_3$, Table VI listing pseudo-first-order rate constants for reactions of the butatriene-bridged diiron hexacarbonyl complexes, and a summary table of chemical analyses (29 pages). Ordering information is given on any current masthead page.

References and Notes

(1) (a) Based in part on the Ph.D. thesis of J.N.G., University of California at Riverside, 1974. (b) To whom correspondence should be addressed at the Technical Center, Union Carbide Corp., South Charleston, W.Va. 25303.
(2) P. C. Ellgen and J. N. Gerlach, *Inorg. Chem.*, **12**, 2526 (1973).
(3) P. C. Ellgen and J. N. Gerlach, *Inorg. Chem.*, **13**, 1944 (1974).
(4) J. N. Gerlach, S. L. McMullin, and P. C. Ellgen, *Inorg. Chem.*, **15**, 1232 (1976).
(5) D. Bright and O. S. Mills, *J. Chem. Soc., Dalton Trans.*, 2465 (1972).
(6) L. F. Dahl and C. F. Wei, *Inorg. Chem.*, **2**, 328 (1963).
(7) R. J. Doedens, *Inorg. Chem.*, **7**, 2323 (1968); **9**, 429 (1970).
(8) R. D. Adams, F. A. Cotton, W. R. Cullen, D. L. Hunter, and L. Mihichuk, *Inorg. Chem.*, **14**, 1395 (1975).
(9) R. B. King and J. J. Eisch, Ed., "Organometallic Synthesis", Vol. I, Academic Press, New York, N.Y., 1965, p 93.
(10) W. McFarlane and G. Wilkinson, *Inorg. Synth.*, **8**, 181 (1966).
(11) A. Zweig and A. K. Hoffman, *J. Am. Chem. Soc.*, **84**, 3278 (1962).
(12) K. K. Joshi, *J. Chem. Soc. A*, 594 (1966).
(13) C. N. R. Rao, "Chemical Applications of Infrared Spectroscopy", Academic Press, New York, N.Y., 1963, p 50.
(14) The programs used were local modifications of Eiss' REDAT for data reduction; Zalkin's FORDAP for Patterson and electron density maps; Busing, Levy, and Martin's ORFLS for least-squares refinement; Johnson's ORTEP for drawings; and Wood's MGEOM for distances, angles, and planes.
(15) The function minimized in the least-squares refinement is $\sum w(|F_o| - |F_c|)^2$ where $w = 4F^2/L^2\sigma(I)$, L is the reciprocal Lorentz–polarization correction, and $\sigma(I) = [P + (t/20)^2B + (0.045I)^2]^{1/2}$. P is the peak count, t is the time spent scanning the peaks in seconds, B is the background count, and I is the integrated intensity: see P. W. R. Corfield, R. J. Doedens, and J. A. Ibers, *Inorg. Chem.*, **6**, 197 (1967).
(16) The atomic scattering factors for Fe(0), P(0), C(0), and H(0) were used in the refinement: J. A. Ibers in "International Tables for X-Ray Crystallography", Vol. III, Kynoch Press, Birmingham, England, 1962, p 202, Table 3.3.1.A.
(17) D. H. Templeton in "International Tables for X-Ray Crystallography", Kynoch Press, Birmingham, England, p 215, Table 3.3.2.C.
(18) $R_1 = \sum||F_o| - |F_c||/\sum|F_o|$ and $R_2 = (\sum w(|F_o| - |F_c|)^2/\sum wF_o^2)^{1/2}$.
(19) Compare with Fe–Fe distances reported in ref 5–7.
(20) P. C. Ellgen and S. L. McMullin, *Inorg. Chem.*, **12**, 2004 (1973).
(21) M. Basato, *J. Chem. Soc., Dalton Trans.*, 911 (1975).
(22) C. A. Tolman, *J. Am. Chem. Soc.*, **92**, 2956 (1970).
(23) J. M. Miller, *J. Chem. Soc. A*, 828 (1967).
(24) S. R. Su and A. Wojcicki, *J. Organomet. Chem.*, **27**, 231 (1971).
(25) F. Basolo and R. G. Pearson, "Mechanisms of Inorganic Reactions", Wiley, New York, N.Y., 1967, p 145.